Journal of
Synchrotron Radiation

ISSN 0909-0495

Received 6 April 2011
Accepted 14 June 2011

X-ray tomography of morphological changes after freeze/thaw in gas diffusion layers

Junho Je,[a] Jongrok Kim,[a] Massoud Kaviany,[b,c] Sang Young Son[d] and MooHwan Kim[c]*

[a]Department of Mechanical Engineering, Pohang University of Science and Technology, San 31, Hyoja-dong, Namgu, Pohang, Kyoungbuk 790-784, South Korea, [b]Department of Mechanical Engineering, University of Michigan, Ann Arbor, MI 48109, USA, [c]Division of Advanced Nuclear Engineering, Pohang University of Science and Technology, San 31, Hyoja-dong, Namgu, Pohang, Kyoungbuk 790-784, South Korea, and [d]School of Dynamic Systems, University of Cincinnati, Cincinnati, OH 45221, USA. E-mail: mhkim@postech.ac.kr

Liquid water produced in a polymer electrolyte membrane fuel cell experiences a freeze/thaw cycle when the cell is switched off and on while operating at ambient temperatures below freezing. This freeze/thaw cycle permanently deforms the polymer electrolyte membrane fuel cell capillary structures and reduces both the cell life and its ability to generate electric power. The X-ray tomography facility at the Pohang Accelerator Laboratory was used to observe the freeze/thaw effects on the gas diffusion layer (GDL), which is the thickest capillary layer in the cell. Morphological changes in the GDL under a water freeze/thaw cycle were observed. A scenario in which freeze/thaw cycles affect fuel cell performance is suggested based on images from X-ray tomography.

Keywords: X-ray tomography; freeze; thaw; deformation; gas diffusion layer; polymer electrolyte membrane fuel cell.

1. Introduction

A fuel cell is an electrochemical device that converts the binding energy of reactants directly into electricity (and resistive heating). Polymer electrolyte membrane (PEM) fuel cells use a solid-state proton-conducting polymer membrane as the electrolyte and have optimal operating temperatures of 333–353 K. This operating temperature is lower than other fuel cell types, thus requiring a small cooling system for operating and short start up time. PEM fuel cells have a power range from a few watts to several hundred kilowatts and smaller systems. These advantages make it suitable for mobile applications. However, commercial use of PEM fuel cells in vehicles has several problems, one of which is that liquid water in the fuel cells may freeze in the winter. Water can be added as vapor to the reactants, but is mainly produced by the electrochemical reaction. This water is very important to PEM fuel cell operation because proton transport and reactivity are poor and power generation is reduced if there is insufficient water in the polymer electrolyte and catalyst layer (Eikerling *et al.*, 2006). However, during the winter, this water can freeze after a PEM fuel cell is turned off, and the freeze/thaw cycle reduces cell performance and durability (Cho *et al.*, 2003). For this reason, the effects of water freezing and thawing have been visualized using scanning electron microscopy (SEM) (Park *et al.*, 2010; Luo *et al.*, 2010) and optical methods (Ishikawa *et al.*, 2008). However, both these methods are limited in that they can show only surface, not internal, structures. Therefore, PEM fuel cell components are cut to observe their internal change after a freeze/thaw cycle, even though the cutting destroys the component structure. On the other hand, X-ray tomography has been used to view the internal structure of the components (Büchi *et al.*, 2008; Ostadi *et al.*, 2008; Becker *et al.*, 2009; Fishman *et al.*, 2010) and the liquid water (Sinha *et al.*, 2006; Krüger *et al.*, 2011; Moriyama & Inamuro, 2011) in them without damaging them.

In this study the change of morphology of the gas diffusion layer (GDL) was visualized and the porosity change of the GDL was measured non-destructively using the X-ray tomography system at the Pohang Accelerator Laboratory (PAL) at the Pohang University of Science and Technology. The deformation within the GDL was larger than would occur in an operating fuel cell. The amount of water underneath the GDL was larger than is expected in an operating fuel cell, because of the water-filled inlet beneath the GDL. Thus, the volume expansion of water was also greater and caused larger deformation within the GDL than expected from the freezing/thaw cycles in an operating fuel cell. Despite these differences, qualitative understandings of the GDL changes owing to the freeze/thaw cycle emerge. The GDL structures were deformed and kept their deformation after the freeze/thaw cycle. Additionally, the porosity of the GDL increased. A scenario for how the freeze/thaw cycles decreased the fuel cell performance was proposed from these experimental results.

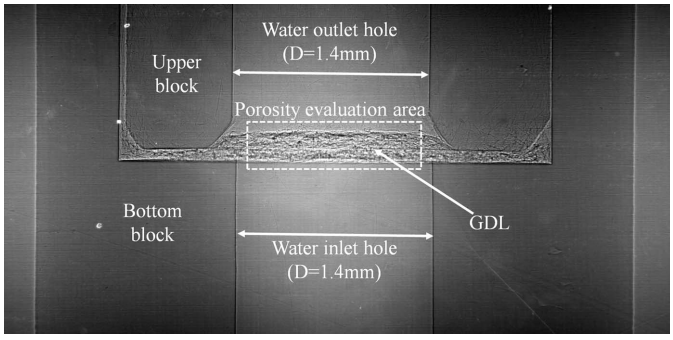

Figure 1
GDL holder for X-ray tomography.

2. Experiments

A device (Fig. 1) was designed to hold the GDL (untreated Toray TGPH 060), which has a general hydrophobic surface behavior, by compressing its edge between two cylindrical blocks. Liquid water was supplied through a 1.4 mm-diameter inlet hole in the lower block. A hole in the upper block was open to the ambient air. First, the structure of a GDL that had never been frozen was visualized. Then, pressurized water was supplied through the inlet hole to the same GDL, and the water pressure was measured. After water had passed through the GDL, the holder, which included the GDL and water, was placed in a freezer to solidify the water. The GDL with the water-filled inlet hole beneath it, when placed in the freezer, caused the water in the GDL pores to ooze out in a topward direction. In an operating fuel cell, water can accumulate in the GDL–MEA (membrane-electrode assembly) interface, since under normal operation this interface is not fully filled with water. Thus, owing to the water under the GDL, for this experiment the expansion is upward and larger, causing larger deformation within the GDL compared with the freezing/thaw cycles in the operating fuel cell. However, we draw some understanding about the freeze/thaw cycles in the fuel cell. After removal from the freezer the water was allowed to thaw and the GDL was blow dried with air and then examined again. The pressurized water was supplied again through the inlet hole until it penetrated the GDL.

A jig was designed to hold the specimen to facilitate microscopic tomography. The sample was attached to a rotating mount and illuminated using the 7B2 X-ray microscopy beamline at PAL. The sample was mounted on a motorized two-axis sample stage. The incident white X-ray beam (photon energy 2.8–5.5 keV) passed through the sample and reached a scintillator that converted the X-rays to visible light. The visible rays reflected off a mirror into a 4008 × 2672 pixel charge-coupled-device camera through a microscope. A 5× lens (5.05 × 3.36 mm field of view) was used because it provided the maximum magnification that allowed visualization of the entire GDL assembly. Tomography was used with the X-ray images (Fig. 1) to reconstruct slices of the GDL (Figs. 2*a* and 2*b*); the intensity profile across a section was measured (Fig. 2*c*).

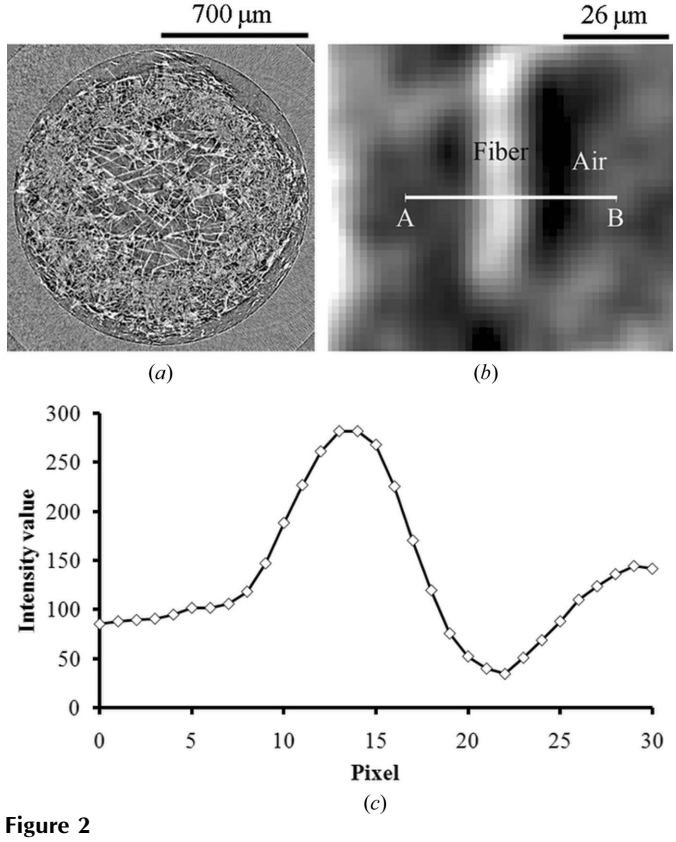

Figure 2
(*a*) Reconstructed X-ray image obtained through tomography, (*b*) close-up of the reconstructed slice, and (*c*) intensity along line AB in (*b*).

3. Results

3.1. GDL lift

Cross-sectional images of the GDL were reconstructed using tomography before and after freeze/thaw (Fig. 3). The increase in water volume during freezing lifted the GDL (Figs. 4*a* and 4*b*) because the bottom side of the hole was closed and the upper side was open to ambient air. The deformed GDL maintained its deformed shape after the ice thawed. This deformation of the GDL after a freeze/thaw cycle (Fig. 3) was consistent with the increase in ohmic and charge-transfer resistances. Freeze/thaw cycles increase the ohmic and charge-transfer resistances of a PEM fuel cell, but do not increase the proton conductivity of the membrane. The increase of the ohmic and charge transfer resistances has been attributed to the increase in the contact resistance in a PEM fuel cell (Cho *et al.*, 2003). From these results, we conjectured what caused the increased resistance.

As a PEM fuel cell operates, water collects in the interface between layers (Nam *et al.*, 2009; Hartnig *et al.*, 2009) (Fig. 5*a*). If this water freezes, it can lift the GDL under the channel as in Fig. 4(*b*). This process may deform the MEA and its interfaces, and may perhaps increase the electrical contact resistance and/or decrease electrochemical reactions. However, this possibility was not considered in this study. The deformation persisted after a freeze/thaw cycle, so a gap remained between the GDL and the MEA (Fig. 5*b*). During subsequent opera-

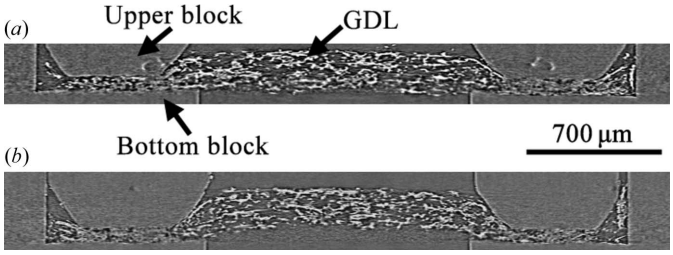

Figure 3
Dried GDL (*a*) before and (*b*) after the freezing/thaw cycle.

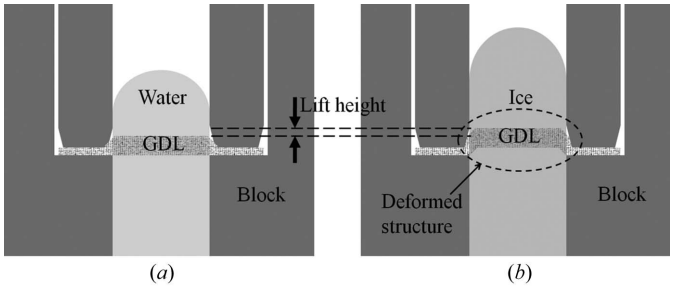

Figure 4
Schematic diagram of (*a*) a GDL before freezing and (*b*) the deformation of a GDL by the freezing of water after freezing.

tion, more water collects in this gap (Fig. 5*c*). When this cell freezes again, the GDL is lifted once more and the gap becomes larger (Fig. 5*d*). Indeed, the gap size increases at an increasing rate because more water collects in the gap as the freeze/thaw cycle is repeated. The increase in the gap continues until the lift force owing to the frozen water exceeds the strength of the GDL. Over a number of freeze/thaw cycles, the contact resistance also increases at a rate that increases with the number of freeze/thaw cycles. Moreover, water collected in the gap covers the surface of the electrodes and blocks the gaseous fuel flow. These processes are consistent with the measurements of the current density of the operating cell and the resistance of PEM fuel cells after freeze/thaw cycles (Cho *et al.*, 2003).

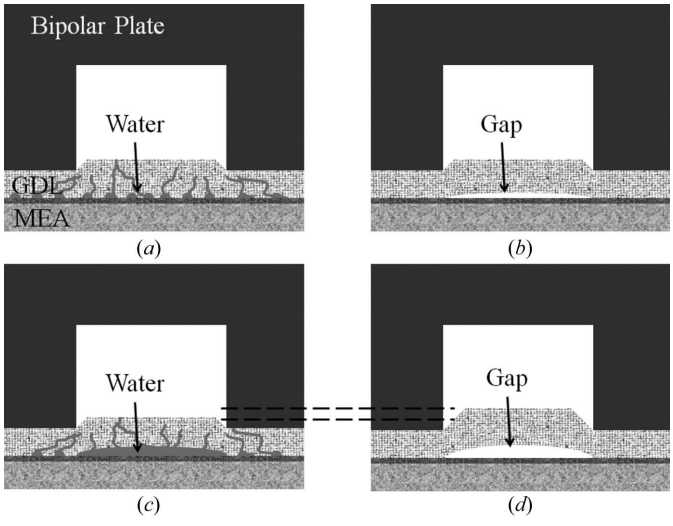

Figure 5
Schematic diagram of GDL deformation due to freezing water in a PEM fuel cell showing (*a*) the GDL in operation before freezing, (*b*) the gap after one freeze/thaw cycle, (*c*) the GDL in operation after several freeze/thaw cycles, and (*d*) the gap after several freeze/thaw cycles.

3.2. Porosity increase and break-through pressure drop

The local porosity distributions of the GDL before and after freezing (Fig. 6) were calculated from the pixel fraction of fiber of the reconstructed slice images (Fig. 2*a*) in the porosity evaluation area (Fig. 1). If the pixel had a higher intensity value than a given threshold, we recognized the pixel where the fiber was located. The fraction depended on the threshold value, so this was important for accurate analysis. We used the threshold porosity of TGPH-060 ($\varepsilon = 0.78$) reported by Toray for the case before freezing. The total volume of fiber was used to calculate the threshold value for the case after freezing. We assumed that the total fiber volume was the same before and after freezing. The threshold value that gave the same total volume of GDL fiber before freezing was then applied after freezing.

The average GDL porosities (0.78 and 0.83 for before and after freezing) and their distributions showed that the porosity increased after freezing. Increased porosity means that the freeze/thaw process made larger pores. Generally, large pores have lower surface tension and resistance to liquid mass transfer than small pores. Thus, this change could increase the removal of any water present in each cell layer. Additionally, the break-through pressure, which is the pressure required for the water to penetrate the GDL, was 3.7 kPa before freezing, but only 0.5 kPa after freezing. This lower pressure drop (ease of flow) can indicate formation of a crack within the GDL. The larger pores and break-through pressure drop reduced the humidity in the catalyst layer and the membrane, and in turn lowered the humidity of the membrane and increased the durability of the catalyst layers (Borup *et al.*, 2006) while decreasing the membrane proton conductivity (Eikerling *et al.*, 2006; Zawodzinski *et al.*, 1993). Thus, we cannot be certain

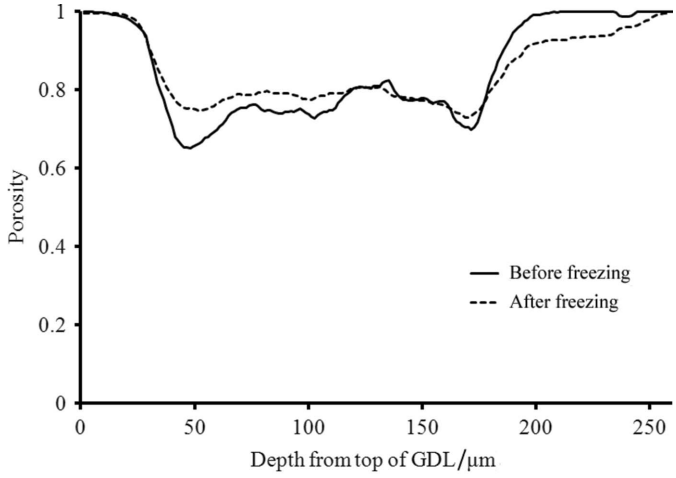

Figure 6
Local porosity of the GDL before and after freezing. The top of the GDL is set to the 0-point.

whether improving water drainage enhances the performance (*i.e.* increases power and durability) of PEM fuel cells or decreases it. Moreover, because water fills large pores more readily than small pores, freezing can reduce the number of empty pores. Empty pores are routes through which gaseous fuel moves to the catalyst layer; thus, we suggest that the increased porosity reduces the number of gaseous fuel routes, and this reduces power generation by PEM fuel cells.

4. Conclusion

In this study the structures and porosities of a GDL before and after water freezing were visualized by X-ray tomography without cutting, which can destroy the GDL structure. Though the freezing condition was extreme to accelerate GDL deformation during the freeze/thaw cycle, the results gave clues to understanding fuel cell degradation by freeze/thaw cycles.

The GDL was deformed by the volume expansion of the frozen water, and this deformation persisted after the water thawed. From this result we suppose that freeze/thaw cycles can cause a gap between the catalyst layer and the GDL. This gap may explain why the power generation of PEM fuel cells is reduced after freeze/thaw cycles. After freezing, the porosity of the GDL increased and the break-through pressure decreased. This increased porosity means pores became larger than the initial condition. The larger pores reduce humidity in PEM fuel cells, and this has both positive and negative effects on PEM fuel cell power generation.

This research was supported by the WCU (World Class University) program through the National Research Foundation of Korea funded by the Ministry of Education, Science and Technology (R31-30005) and the National Research Foundation of Korea (NRF) through a grant provided by the Korean Ministry of Science and Technology (MOST), M60602000005-06E0200-00410.

References

Becker, J., Flückiger, R., Reum, M., Büchi, F. N., Marone, F. & Stampanoni, M. (2009). *J. Electrochem. Soc.* **156**, B1175–B1181.
Borup, R. L., Davey, J. R., Garzon, F. H., Wood, D. L. & Inbody, M. A. (2006). *J. Power Sources*, **163**, 76–81.
Büchi, F. N., Flückiger, R., Tehlar, D., Marone, F. & Stampanoni, M. (2008). *ECS Trans.* **16**, 587–592.
Cho, E. A., Ko, J. J., Ha, H. Y., Hong, S. A., Lee, K. Y., Lim, T. W. & Oh, I. H. (2003). *J. Electrochem. Soc.* **150**, A1667–A1670.
Eikerling, M., Kornyshev, A. A. & Kucernak, A. P. (2006). *Phys. Today*, **59**, 38–44.
Fishman, Z., Hinebaugh, J. & Bzylak, A. (2010). *J. Electrochem. Soc.* **157**, B1643–B1650.
Hartnig, C., Manke, I., Kuhn, R., Kleinau, S., Goebbels, J. & Banhart, J. (2009). *J. Power Sources*, **188**, 468–474.
Ishikawa, Y., Hamada, H., Uehara, M. & Shiozawa, M. (2008). *J. Power Sources*, **179**, 547–552.
Krüger, P., Markötter, H., Haussmann, J., Klages, M., Arlt, T., Banhart, J., Hartnig, C., Manke, I. & Scholta, J. (2011). *J. Power Sources*, **196**, 5250–5255.
Luo, M., Huang, C., Liu, W., Luo, Z. & Pan, M. (2010). *Intl J. Hydrogen Energy*, **35**, 2986–2993.
Moriyama, K. & Inamuro, T. (2011). *Commun. Comput. Phys.* **9**, 1206–1218.
Nam, J. H., Lee, K. J., Hwang, G. S., Kim, C. J. & Kaviany, M. (2009). *Intl J. Heat Mass Transfer*, **52**, 2779–2791.
Ostadi, H., Jiang, K. & Prewett, P. D. (2008). *Micro Nano Lett.* **3**, 106–109.
Park, G. G., Lim, S. J., Park, J. S., Yim, S. D., Park, S. H., Yang, T. H., Yoon, Y. G. & Kim, C. S. (2010). *Curr. Appl. Phys.* **10**, S62–S65.
Sinha, P. K., Halleck, P. & Wang, C. Y. (2006). *Electrochem. Solid-State Lett.* **9**, A344–A348.
Zawodzinski, T. A. Jr, Derouin, C., Radzinski, S., Sherman, R. J., Smith, V. T., Springer, T. E. & Gottesfeld, S. (1993). *J. Electrochem. Soc.* **140**, 1041–1047.